Chapter 6

Structural Characterisation of $Ba_2NdSn_xSb_{1-x}O_{6-\delta}$

6.1 Introduction

As discussed in Chapter 1 oxygen deficient perovskites are of significant interest to material scientists because of their high ionic and electronic conductivity[1-4]. Ionic conductivity in such perovskites typically takes the form of oxygen anion or proton conductivity with some materials, such as $BaLn_xCe_{1-x}O_3$[5] and $Ba_2YSnO_{5.5}$[6], exhibiting both types. Typically such materials have high proton conductivity at intermediate temperatures under humid environments and greater oxygen anion conductivity at higher temperatures in dry environments[7]. $Ba_2YSnO_{5.5}$ is a rare example of a double perovskite known to have good ionic conducting properties and studies of similar double perovskites are also likely to show interesting results. In particular similar series where the amount of oxygen anion vacancies in the structure is reduced, by for example doping the Sn^{4+} site with a B'^{5+} cation, are of interest because it is likely that this will lead to more stable materials under reducing conditions[6].

In Chapter 5 it was shown that in the series $Ba_2LnSn_xB'_{1-x}O_{6-\delta}$ (Ln = Pr or Tb and B' = Nb^{5+} or Sb^{5+}) the Ln^{3+} cations undergo an oxidation state change to Ln^{4+} as x increases. Results obtained from analysis of XANES spectra suggest that these compounds have very little or no oxygen anion vacancies and are therefore likely to have limited ionic conductivity. In this chapter the synthesis and structural analysis of the series $Ba_2NdSn_xSb_{1-x}O_{6-\delta}$ is carried out. Nd^{3+}, unlike Pr^{3+} or Tb^{3+} can not be oxidised to a tetravalent oxidation state meaning that increased Sn^{4+} doping of the B' site must lead to increased oxygen anion vacancies[8]. Such an increased level of oxygen vacancies is likely to lead to an increase in the overall ionic conductivity of these materials.

The series $Ba_2NdSn_xSb_{1-x}O_{6-\delta}$ was selected for study, rather than the analogous Y^{3+} compounds, since the larger ionic radius of Nd^{3+} (cf. an ionic radius of 0.98 Å for

Nd^{3+} to 0.90 Å for Y^{3+}[9]) suggests that these are more likely to adopt lower symmetry structures. Lower symmetry perovskite structures are in interest to this work because of the potential for oxygen anion vacancy ordering in structures with crystallographically distinct oxygen sites. Preferential occupancy of the oxygen vacancies could have a significant effect on the pathway of oxygen anion conductivity and lead to ionic conductivity being higher along one axis or plane of the crystal structure than along another. To date most studies of octahedrally tilted oxygen deficient perovskites with more than one oxygen anion site have indicated that oxygen vacancies tend to concentrate on the equatorial sites of the BO_6 octahedra[10-13]. How any ordering present in these materials changes with temperature is fundamental to the role it may play in their application in devices such as solid oxide fuel cells.

To explore the structures of compounds in the series $Ba_2NdSn_xSb_{1-x}O_{6-\delta}$ suitable samples have been synthesised and structurally characterised using synchrotron X-ray and neutron diffraction. Neutron diffraction is particularly critical to this study because of the relatively high sensitivity of this technique to lighter elements, such as oxygen, compared to X-ray diffraction. This higher sensitivity makes the determination of the extent of any oxygen anion ordering present possible, particularly when neutron diffraction data is collected to low *d*-space.

6.2 Synthesis of $Ba_2NdSn_xSb_{1-x}O_{6-\delta}$

Samples of $Ba_2NdSn_xSb_{1-x}O_{6-\delta}$ (x = 0, 0.1, 0.2,…, 1) were synthesised from stoichiometric mixtures of $BaCO_3$, Nd_2O_3, SnO_2 and Sb_2O_3. After being finely ground in an acetone slurry the samples were heated at 800 °C for 24 hrs. After being reground the samples were sequentially heated at 1000, 1100, 1150, 1200, 1300, 1350 and 1400 °C for periods of 24 hrs with samples being reground between each heating period. Where required samples were then heated for up to 96 hrs at 1450 °C to improve their purity and crystallinity. Where x = 0.6, 0.8 and 1.0 the larger samples (~ 10-15 g) required for neutron diffraction were heated above 1350 °C in a platinum crucible to prevent the possibility of these Sn^{4+} rich samples reacting with the vessel in which they were held. Another large sample (~ 15g) of $Ba_2NdSnO_{5.5}$ was also synthesised, with this sample being held in an alumina crucible for all steps of the

heating schedule. It should be noted that all samples used for neutron diffraction were dried by heating overnight at 1000 °C prior to analysis in order to eliminate any water present in the structure of these compounds.

A second large sample (~ 10g) of $Ba_2NdSn_{0.6}Sb_{0.4}O_{5.7}$ was synthesised using the aforementioned procedure and, after drying, was placed on a Schlenk line under vacuum for three days to ensure any trace quantities of water present was removed. The compound was then exposed for a day to an atmosphere of Argon, which had been humidified using D_2O, to deuterate the sample. The sample was then transferred to a glove box and sealed in a glass vial under an atmosphere of Argon to minimise any exchange of H_2O for D_2O while the compound was being taken to the ISIS facility in the United Kingdom.

6.3 Experimental Method

Synchrotron X-ray diffraction patterns were collected using the Debye-Scherrer diffractometer at the ANBF, beamline 20B at the Photon Factory as described in Section 2.2.2.1. Diffraction patterns were collected at room temperature using 0.80088(1), 0.80123(1) or 0.80286(1) Å X-rays. Following this diffraction patterns of $Ba_2NdSn_{0.3}Sb_{0.7}O_{5.85}$ and $Ba_2NdSnO_{5.5}$ were collected above ambient temperature up to a maximum temperature of 800 °C using the custom built furnace and employing 0.80088(1) and 0.80123(1) Å X-rays respectively.

Time-of-flight neutron diffraction patterns of $Ba_2NdSn_xSb_{1-x}O_{6-\delta}$ (x = 0, 0.2, 0.3, 0.6, 0.8 and 1.0) and the deuterated sample of $Ba_2NdSn_{0.6}Sb_{0.4}O_{5.7}$ were collected at room temperature using the Polaris diffractometer at the ISIS facility (as described in Section 2.2.3.4). Diffraction patterns of $Ba_2NdSn_{0.6}Sb_{0.4}O_{5.7}$ and $Ba_2NdSnO_{5.5}$ were also collected above ambient temperature, up to a maximum temperature of 1000 °C. Neutron diffraction patterns of both the deuterated and dried samples of $Ba_2NdSn_{0.6}Sb_{0.4}O_{5.7}$ were also collected at –269 °C (4 K). Samples were held in vanadium cans during the measurements. Special care was taken when transferring the deuterated sample of $Ba_2NdSn_{0.6}Sb_{0.4}O_{5.7}$ into its can to minimise the possibility of any exchange of D_2O with the atmosphere. The transfer was carried out in a glove

bag under an atmosphere of N_2 with a piece of indium metal being used to improve the quality of the seal between the sample can and lid. The sample cans were mounted in an AS Scientific "Orange" helium cryostat to collect patterns below ambient temperature. For measurements above ambient temperature a RAL vacuum furnace was used. This furnace had vanadium heating elements with thermometry based on a K-type thermocouple positioned in contact with the sample can above the beam. Variable temperature patterns were collected over the temperature range of 100 to 1000 °C in 50° steps. The patterns were recorded for a total incident proton beam current of between 125 and 250 μAh, as required, and refinements carried over the *d*-space range of 0.25 to 3.18 Å.

X-ray Absorption Near-Edge Structure (XANES) spectra of the L-edges of the Sn^{4+} and Sb^{5+} cations in $Ba_2NdSn_xSb_{1-x}O_{6-\delta}$ (x = 0, 0.2, 0.3, 0.6, 0.8 and 1.0)) were collected using beamline 16A1 at the NSRRC (see Section 2.4.2) using a single scan over the energy range of 3.779-4.998 keV.

6.4 Results and Discussion

As expected from the results presented in Chapter 3 the synchrotron X-ray diffraction pattern of Ba_2NdSbO_6 indicated that it adopts $R\bar{3}$ rhombohedral symmetry (tilt system $a^-a^-a^-$) with a good fit being obtained to the pattern using a model with this structure. Visual examination of the X-ray diffraction pattern of $Ba_2NdSnO_{5.5}$ revealed that the peaks that correspond to the (444) and (800) reflections of the cubic perovskite structure were asymmetric suggesting splitting of these peaks that could not be fully resolved (see Figure 6.1). This is consistent with monoclinic symmetry. Since the only super-lattice reflections that were observed were *R*-point reflections, indicative of cation-ordering and/or out-of-phase tilting, the compound was assigned as having *I*2/*m* symmetry. To obtain an adequate fit to this diffraction pattern, however, a slightly unusual metric cell was required that had a *b*-axis slightly longer than the *a*-axis (see Figure 6.2 and Table 6.1 for unit cell parameters presented in graphical and tabulated forms respectively). This is different from most monoclinic perovskites examined in this thesis and in other studies where the *a*-axis is the longest[14, 15]. A good fit was obtained using a structure with this unit cell (R_p and R_{wp}

of 4.8 and 5.4 % respectively), which accounted for all the observed reflections in the diffraction pattern and had a significant monoclinic angle (β = 90.098(2)°). This confirms that despite $Ba_2NdSnO_{5.5}$ possessing an unusual unit cell it is, at ambient temperature, in all likelihood *I*2/*m* monoclinic.

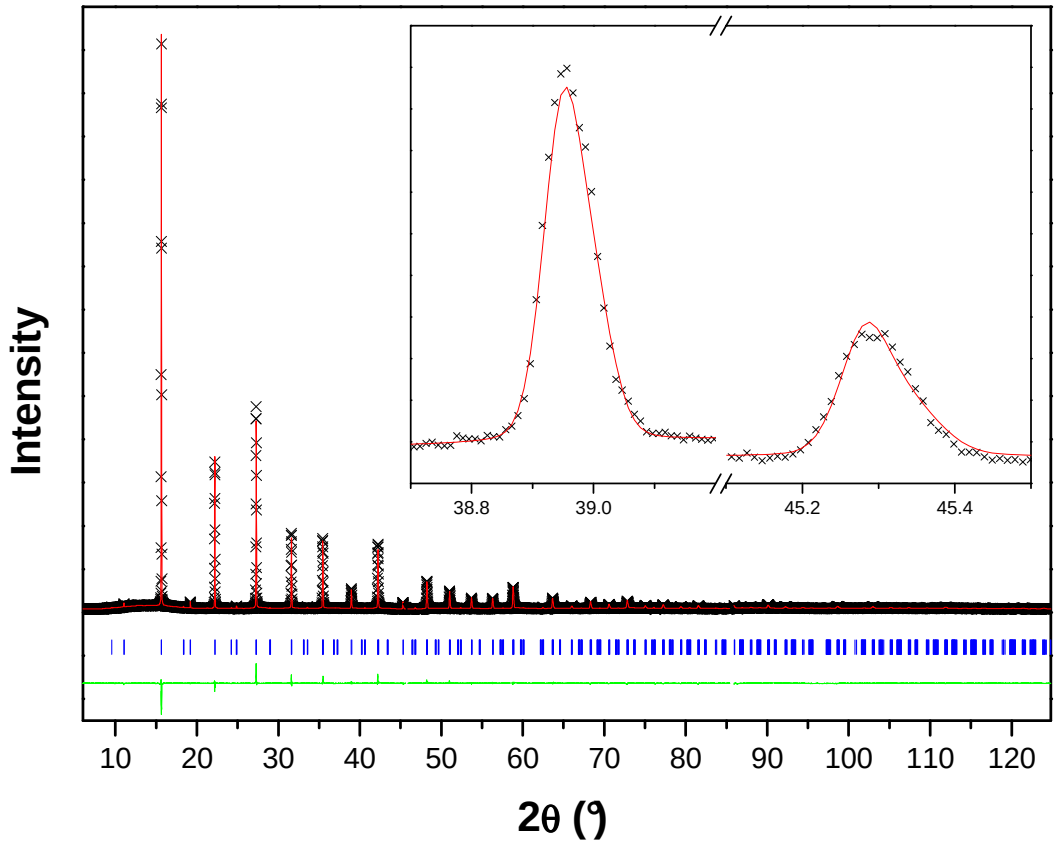

Figure 6.1: Synchrotron X-ray diffraction pattern of $Ba_2NdSnO_{5.5}$ at ambient temperature. The crosses, upper and lower continuous lines represent the observed and calculated intensities and the difference between these respectively. The vertical markers show the positions of the allowed Bragg reflections. The inset indicates asymmetry indicative of unresolved splitting of the peaks corresponding to the (444) and (800) reflections of the cubic perovskite indicating that monoclinic symmetry is adopted.

Synchrotron X-ray diffraction patterns of compounds in the series $Ba_2NdSn_xSb_{1-x}O_{6-\delta}$ with x = 0.6-0.9 were also well fitted by models with *I*2/*m* symmetry as illustrated in Figure 6.3. The samples where x = 0.1 and 0.2 were found to be $R\bar{3}$ rhombohedral, similar to Ba_2NdSbO_6, with the X-ray diffraction patterns of these compounds being well fitted by this structure. The diffraction patterns of samples with x = 0.3-0.5,

however, were not well fitted by single phase models in either *I*2/*m* or $R\bar{3}$ with a refinement consisting of a combination of these two structures being necessary to obtain an adequate fit to these diffraction patterns. The unit cell volume of the rhombohedral structure is observed to decrease slightly with increasing x (see Table 6.1). This is somewhat unusual since Sn^{4+} has a larger ionic radius than Sb^{5+} (cf. an ionic radius of 0.69 Å for Sn^{4+} to 0.60 Å for Sb^{5+}[9]) and it would be expected that the unit cell volume should increase with increasing Sn^{4+} doping as found for the monoclinic structures. It is not clear why this trend is observed although it may be related to the presence of a smaller number of oxygen vacancies in the rhombohedral samples compared to the *I*2/*m* monoclinic compounds.

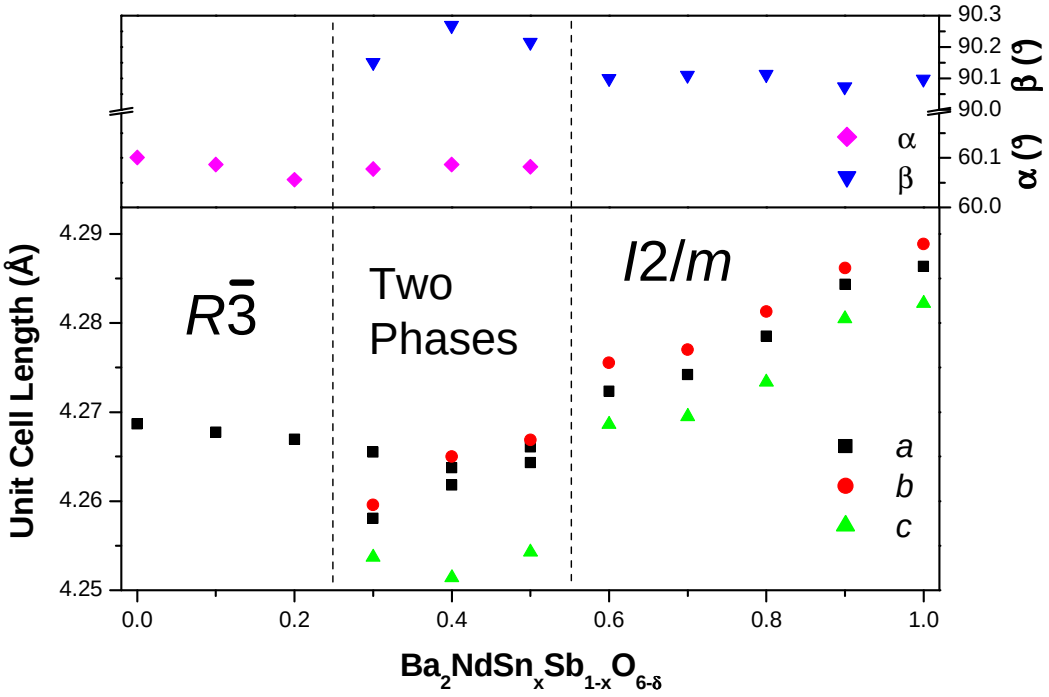

Figure 6.2: Lattice parameters for compounds in the series $Ba_2NdSn_xSb_{1-x}O_{6-\delta}$ determined using synchrotron X-ray diffraction. Unit cell lengths have been reduced to the size of the primitive cubic perovskite for ease of comparison. It should be noted that the lattice parameters determined for samples with x = 0, 0.6 and 1.0 were determined using different wavelengths than the other samples.

Table 6.1: Phase composition and unit cell parameters for the $Ba_2NdSn_xSb_{1-x}O_{6-\delta}$ series of compounds determined using synchrotron X-ray diffraction.

x	Space Group	*a* (Å)	*b* (Å)	*c* (Å)	α (°)	β (°)	Volume (Å^3)	Phase Composition (mol %)
0	$R\bar{3}$	6.03682(1)	= *a*	= *a*	60.1003(2)	= α	155.917(15)	100
0.1	$R\bar{3}$	6.03551(3)	= *a*	= *a*	60.0867(5)	= α	155.768(31)	100
0.2	$R\bar{3}$	6.03440(6)	= *a*	= *a*	60.0558(10)	= α	155.574(69)	100
0.3	$R\bar{3}c$	6.03233(9)	= *a*	= *a*	60.0776(13)	= α	155.489(86)	83.9(4)
	*I*2/*m*	6.02183(40)	6.02399(41)	8.50743(38)	90	90.1505(32)	308.609(31)	16.1(2)
0.4	$R\bar{3}c$	6.02988(10)	= *a*	= *a*	60.0865(23)	= α	155.344(151)	65.6(5)
	*I*2/*m*	6.02715(28)	6.03163(30)	8.50286(16)	90	90.2269(26)	309.106(22)	34.4(4)
0.5	$R\bar{3}c$	6.03319(26)	= *a*	= *a*	60.0822(38)	= α	155.573(257)	38.9(7)
	*I*2/*m*	6.03064(21)	6.03430(22)	8.50860(15)	90	90.2148(17)	309.632(17)	61.1(8)
0.6	*I*2/*m*	6.04200(10)	6.04052(10)	8.53724(11)	90	90.1003(14)	311.891(8)	100
0.7	*I*2/*m*	6.04465(6)	6.04863(5)	8.53900(5)	90	90.1100(6)	312.201(4)	100
0.8	*I*2/*m*	6.05076(7)	6.05465(7)	8.54670(7)	90	90.1126(8)	313.110(6)	100
0.9	*I*2/*m*	6.05895(6)	6.06159(6)	8.56100(6)	90	90.0731(9)	314.418(5)	100
1.0	*I*2/*m*	6.06182(15)	6.06539(14)	8.56439(11)	90	90.0977(17)	314.889(11)	100

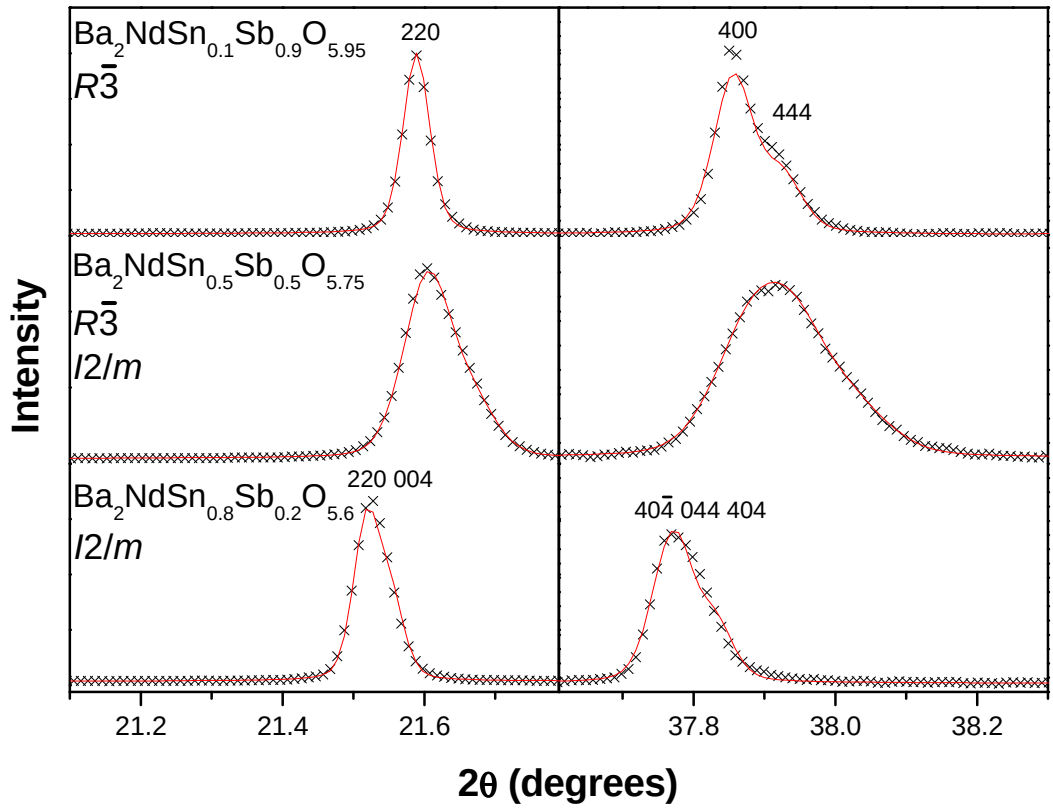

Figure 6.3: Selected portions of synchrotron X-ray diffraction patterns of compounds in the series $Ba_2NdSn_xSb_{1-x}O_{6-\delta}$ indicating the various structures adopted. The crosses and the continuous line represent the observed and calculated intensities, respectively. The patterns have been rescaled to better illustrate the changes, with the parent (444) reflection near $2\theta = 38.0°$ being ~ $1/5^{th}$ as intense as the cubic (400) reflection near $2\theta = 21.6°$.

The two phase region found in the series $Ba_2NdSn_xSb_{1-x}O_{6-\delta}$ could arise from either a discontinuous phase transition between monoclinic and rhombohedral symmetry, as required by group theory[16], or a compositional difference between these two phases. Therefore variable temperature synchrotron X-ray diffraction patterns were collected of $Ba_2NdSn_{0.3}Sb_{0.7}O_{5.85}$ up to a maximum temperature of 800 °C. These patterns showed that this sample consisted of two phases up to the maximum temperature examined (see Figure 6.4), where it was well fitted by two cubic structures (R_p and R_{wp} of 3.5 and 4.7 %). The persistence of the two phase region over such a large temperature range indicates that the co-existence of these phases is caused by phase segregation, similar to that found in $Ba_2NdNb_{1-x}Sb_xO_6$ and $Ba_2PrSn_xSb_{1-x}O_{6-\delta}$ in Chapters 4 and 5 respectively, and not as a result of a phase transition. A combination

of Scanning Electron Microscopy (SEM) and Energy Dispersive X-ray (EDX) analysis, however, did not find any evidence of cation segregation with only a small variation in the composition of the different regions being found in both the single and multi-phase samples (see Figure 6.5 for secondary and backscattered electron images). This suggests that whatever segregation is present occurs on a smaller scale, either compositionally or spatially, than can be readily examined using SEM and EDX analysis. EDX analysis of this series may be complicated further by the overlap of the Sn^{4+} and Sb^{5+} X-ray emission spectra.

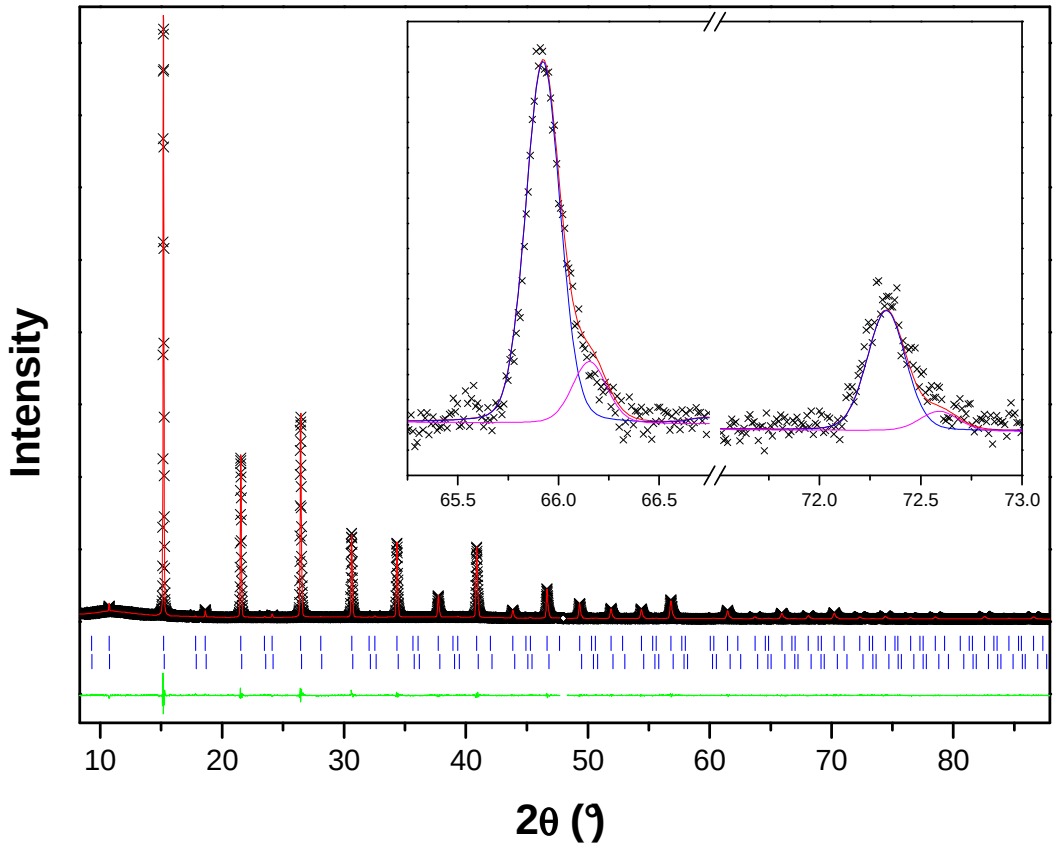

Figure 6.4: Synchrotron X-ray diffraction pattern of $Ba_2NdSn_{0.3}Sb_{0.7}O_{5.85}$ at 800 °C. The format is the same as for Figure 6.1. The insert depicts the calculated intensities of the two cubic phases in the sample and the overall calculated intensity.

Having determined the ambient temperature structures of the compounds in the series $Ba_2NdSn_xSb_{1-x}O_{6-\delta}$, a variable temperature synchrotron X-ray diffraction study of $Ba_2NdSnO_{5.5}$ was carried out to examine its structure above ambient temperature. While it was found that this sample maintained *I*2/*m* monoclinic symmetry up to 800 °C, the maximum temperature examined in this work, an unusual contraction of

the lattice parameters was observed between 250 and 500 °C (see Figure 6.6). This remarkable behaviour was not repeated on cooling from 800 °C suggesting that this compound does not truly exhibit negative thermal expansion. Evidently this contraction is caused by a change in the crystal structure of this material on heating, which is not reversed on cooling. Since the related compound $Ba_2YSnO_{5.5}$ is known to be a good proton conductor[6] and proton conductors absorb water into their crystal structures it is likely that the decrease of the unit cell volume of $Ba_2NdSnO_{5.5}$ upon heating is caused by the loss of water present in the structure[17-21].

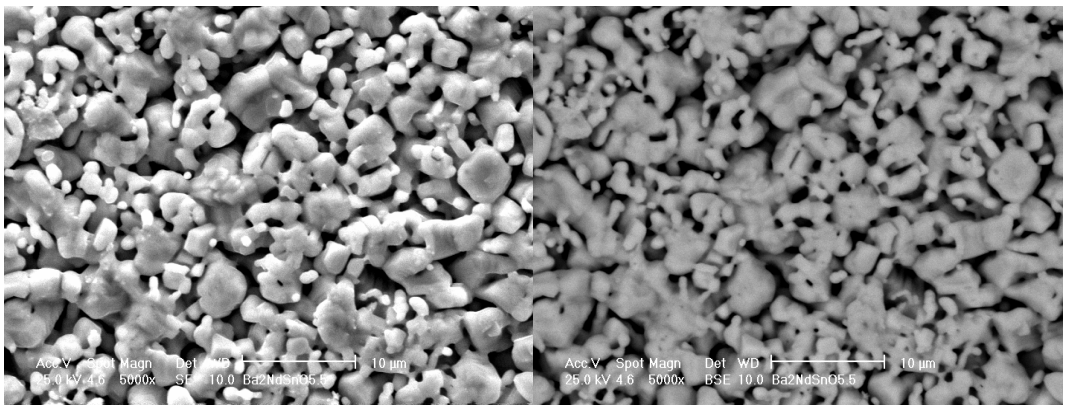

Figure 6.5: Secondary (left) and backscattered (right) electron images of the single phase sample $Ba_2NdSnO_{5.5}$. The lack of contrast in the backscattered electron image suggests that this sample is homogeneous.

Thermogravimetric Analysis (TGA), measured under an inert atmosphere of N_2 by David Cassidy at ANSTO, indicates that there are three regions of significant weight loss for this sample of $Ba_2NdSnO_{5.5}$ upon heating (see Figure 6.7). The first of these is below 100 °C and is expected to be associated with the loss of water bound to the surface of this compound. The second and third regions are between 200 and 450 °C and 500 and 625 °C, respectively, and most likely arise as a result of the loss of water from the crystal structure. These regions of weight loss coincide well with features apparent in the diffraction studies upon heating. TGA showed a total weight loss equivalent to 0.72 moles of water per mole of $Ba_2NdSnO_{5.5}$ over these two regions. This is a remarkable result since the water was absorbed into this sample from the air while sitting in a closed vial at ambient temperature.

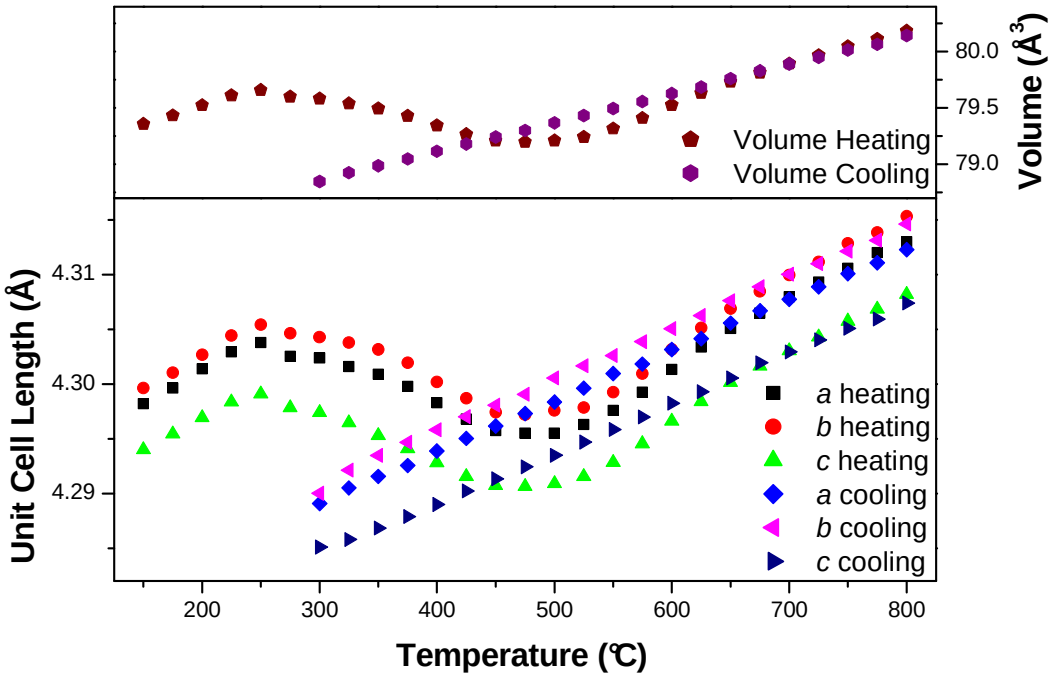

Figure 6.6: Reduced lattice parameters and unit cell volume of $Ba_2NdSnO_{5.5}$ versus temperature.

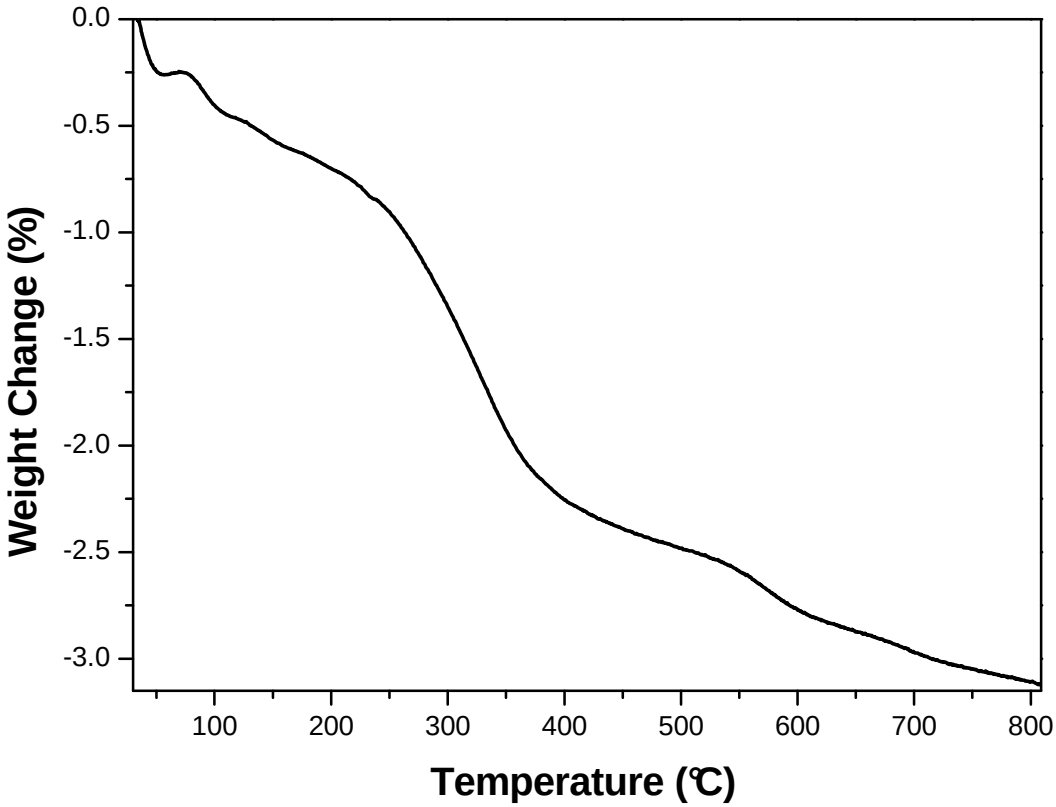

Figure 6.7: Weight loss versus temperature plot for $Ba_2NdSnO_{5.5}$ in an atmosphere of N_2. The weight loss in the regions of 200-450 °C and 500-625 °C is 1.69 and 0.35 % respectively.

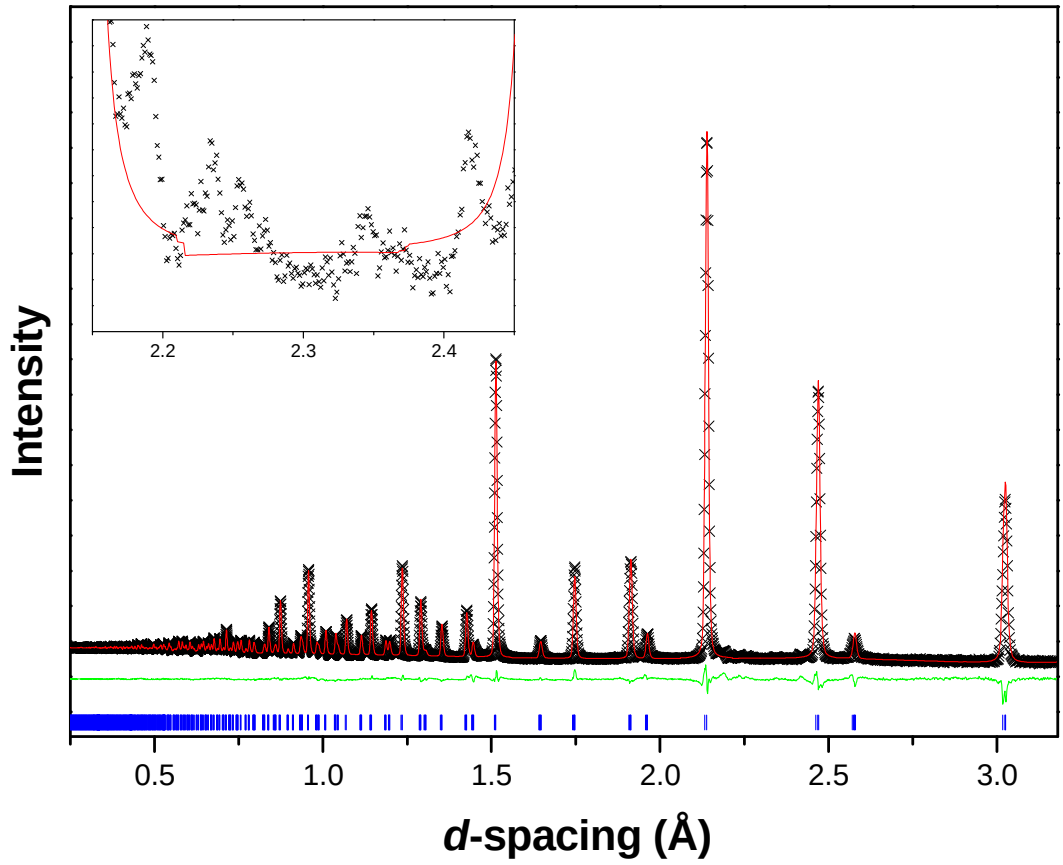

Figure 6.8: Ambient temperature neutron diffraction pattern of the deuterated sample of $Ba_2NdSn_{0.6}Sb_{0.4}O_{5.7}$. The format is the same as for Figure 6.1. The insert indicates the weak peaks revealing the presence of an unidentified impurity.

It would be interesting to locate the precise position of the water in the crystal structure of compounds in the series $Ba_2NdSn_xSb_{1-x}O_{6-\delta}$, particularly since the amount of oxygen in the quantity of water absorbed by $Ba_2NdSnO_{5.5}$ is greater than the number of oxygen vacancies in this sample. Oxygen in water absorbed into a perovskite structure usually fills these vacancies so it is unclear where the remaining oxygen anions might be situated[3, 17, 22]. Attempts to determine the location of D_2O, and in particular the deuterium site, in $Ba_2NdSn_{0.6}Sb_{0.4}O_{5.7}$ were, however, unsuccessful. Neutron diffraction patterns collected of a deuterated sample of $Ba_2NdSn_{0.6}Sb_{0.4}O_{5.7}$ at ambient temperature and -269 °C (4 K) were well fitted by a "dry" *I*2/*m* structure which did not allow for the presence of any deuterium in the compound (see Figure 6.8). The Fourier difference maps calculated from the fits obtained using this "dry" model to the two neutron diffraction patterns obtained of this compound did not reveal any significant additional nuclear density that was

unaccounted for by these refinements. This suggests that there are no additional atoms in the structure of this material that are unaccounted for by this "dry" model indicating that no D_2O was present in the perovskite structure. The unit cell volume of the deuterated sample was determined to be within 0.2 % of the size of the unit cell of the dried $Ba_2NdSn_{0.6}Sb_{0.4}O_{5.7}$ sample at both temperatures examined. This contrasts significantly with the large change in the volume of $Ba_2NdSnO_{5.5}$ found when water is lost from its crystal structure and suggests that the deuterated sample of $Ba_2NdSn_{0.6}Sb_{0.4}O_{5.7}$ contains little or no D_2O.

TGA of the deuterated sample in an atmosphere of N_2, however, revealed a weight loss at elevated temperatures of approximately 0.61 % of total weight over two regions, between 200 and 400 °C and 450 and 560 °C. Due to the care taken to thoroughly dry this sample prior to deuteration it was expected that the sample would only contain heavy water. This weight loss is therefore consistent with the structure of this sample containing 0.19 moles of D_2O per mole of $Ba_2NdSn_{0.6}Sb_{0.4}O_{5.7}$. While this is significantly less than the amount of water found to be absorbed into the structure of $Ba_2NdSnO_{5.5}$ it is expected that any deuterium present in the structure of this compound should be ordered, as is the case for other deuterated perovskites[18-20, 22]. This result, therefore, suggests that there still should have been sufficient deuterium present in this sample to determine the position of the deuterium site.

There are three possible reasons why attempts to determine the deuterium site in this material failed. The first possibility is that the deuterium preferentially segregated into an impurity phase which was shown to be present in the deuterated sample by the presence of several weak un-indexed peaks in the neutron diffraction pattern (see Figure 6.8). The impurity causing these peaks could not be identified and was not present in the dried $Ba_2NdSn_{0.6}Sb_{0.4}O_{5.7}$ sample. These peaks had less than 1 % of the intensity of the most intense peak in the neutron diffraction pattern indicating that only a trace amount of this phase was present. It is, therefore, thought unlikely that it could contain all of the deuterium in the sample. Another possibility is that the seal of the vanadium can was not sufficiently tight to prevent the D_2O escaping from the compound while cooling, under vacuum, in the cryostat. Similarly it is also possible that sufficient H_2O may have exchanged for D_2O in the sample prior to this experiment so that the different scattering lengths of hydrogen and deuterium (cf. a

coherent scattering length of -3.74 fm for H to 6.67 fm for D[23]) led to little or no overall nuclear scattering density from whatever site they occupy in the material. If this last reason is true, however, it is still unlikely that the deuterated sample of $Ba_2NdSn_{0.6}Sb_{0.4}O_{5.7}$ contains a significant amount of water since there was not a significant difference in the unit cell volume of the deuterated and dried samples. Regardless of the reason why the deuterium site in $Ba_2NdSn_{0.6}Sb_{0.4}O_{5.7}$ could not be located it is hoped that future studies of deuterated samples in the series $Ba_2NdSn_xSb_{1-x}O_{6-\delta}$ may lead to the successful identification of this site. It is thought that deuterating samples at elevated temperatures may increase the kinetics of deuterium absorption and thereby increase the amount of deuterium absorbed into the sample[20]. Unfortunately the study of this deuterated sample was delayed for approximately a year due to the shut down of the OPAL reactor in Australia and the ISIS facility and, due to time constraints, it was not possible to repeat this.

Having established that the structure of compounds in the series $Ba_2NdSn_xSb_{1-x}O_{6-\delta}$ changes from $R\bar{3}$ rhombohedral to *I*2/*m* monoclinic with increasing x, neutron diffraction was used to characterise selected samples with a particular focus on determining if oxygen vacancy ordering was present. The neutron diffraction patterns of $Ba_2NdSnO_{5.5}$ exhibited unusually broad and anisotropic peak shape which could not be successfully fitted (see Figure 6.9). This occurred for two samples of $Ba_2NdSnO_{5.5}$ for which neutron diffraction patterns were collected, although the diffraction pattern of the sample heated above 1350 °C in a platinum crucible had somewhat improved peak shape. In contrast with the problems encountered fitting the neutron diffraction patterns of this compound the peak shapes of the synchrotron X-ray diffraction patterns of $Ba_2NdSnO_{5.5}$ were adequately fitted using a pseudo-Voigt peak shape, particularly after a small amount of anisotropic peak broadening was allowed for in peaks with (*hkl*) of the type (00*l*). This suggests that it is the limitations in the peak shape models that can be employed using the GSAS program that prevented the successful fitting of the neutron diffraction patterns. It is thought that the high degree of strain present in $Ba_2NdSnO_{5.5}$, which is responsible for this sample induced peak shape broadening, is most likely induced by the presence of a large number of oxygen vacancies in the structure of this compound.

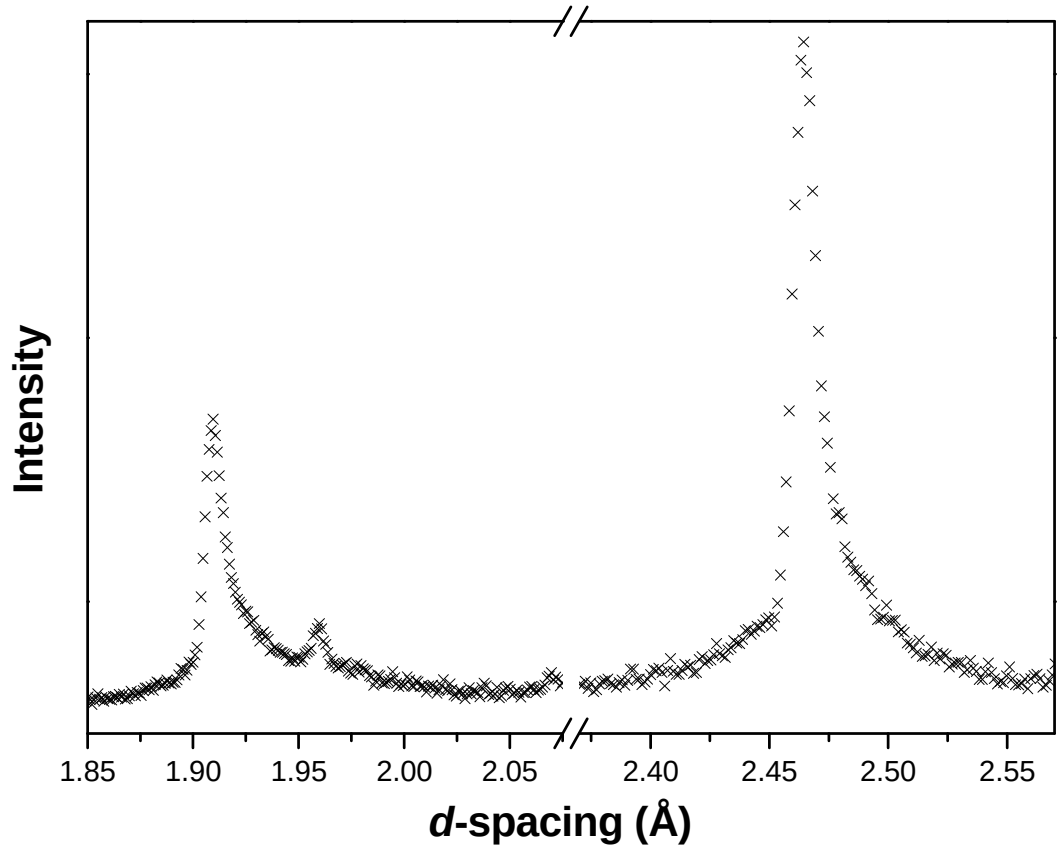

Figure 6.9: Selected portion of the neutron diffraction pattern of $Ba_2NdSnO_{5.5}$ obtained at ambient temperature illustrating the anisotropic peak shape broadening present in this sample.

The neutron diffraction patterns of other compounds examined in the series $Ba_2NdSn_xSb_{1-x}O_{6-\delta}$ were well fitted by either *I*2/*m*, $R\bar{3}$ or a mixture of these phases consistent with the results obtained using X-ray diffraction (see Figure 6.10). There was no indication of any additional peaks, such as *M*- or *X*-point reflections, in these patterns. Bond valencies estimated from the neutron diffraction analysis reveal that the Nd^{3+} cations are overbonded similarly to the lanthanide cations in the compounds examined in Chapters 3 and 5 (see Table 6.2 and 6.3 for crystallographic details and selected bond distances respectively). Despite this overbonding the average Nd-O bond gets shorter with increasing x while the average Sn^{4+}/Sb^{5+}-O bond becomes longer. This is a result of the substitution of the larger Sn^{4+} cation for Sb^{5+} (cf. an ionic radius of 0.69 Å for Sn^{4+} to 0.60 Å for Sb^{5+}[9]) causing the bond length of the mixed Sn^{4+} and Sb^{5+} site to expand requiring the Nd-O bond length to shorten to offset this. The higher number of oxygen vacancies that are present in the more heavily Sn^{4+} doped compounds compensate somewhat for the increased overbonding

of the Nd^{3+} cations. It should be noted that the bond valencies provided in Table 6.3 for the oxygen deficient perovskites have been calculated by multiplying the partial occupancy of each site by the bond valence determined for the appropriate bond length (i.e. for the Nd-O bond in $Ba_2NdSn_{0.2}Sb_{0.8}O_{5.9}$ the bond distance of 2.2902(5) Å yields a bond valence of 3.76 which, when multiplied by the partial occupancy of the oxygen site, gives a bond valence of 3.70). Clearly such an approach has limitations in regards to determining the bond strength of a specific cation in its local environment. Despite this it was considered to be the most appropriate approach for accounting for the partial occupancy of the oxygen sites when calculating bond valencies particularly if, as expected for an ionic conducting perovskite, the oxygen anions are rapidly moving from one position to another.

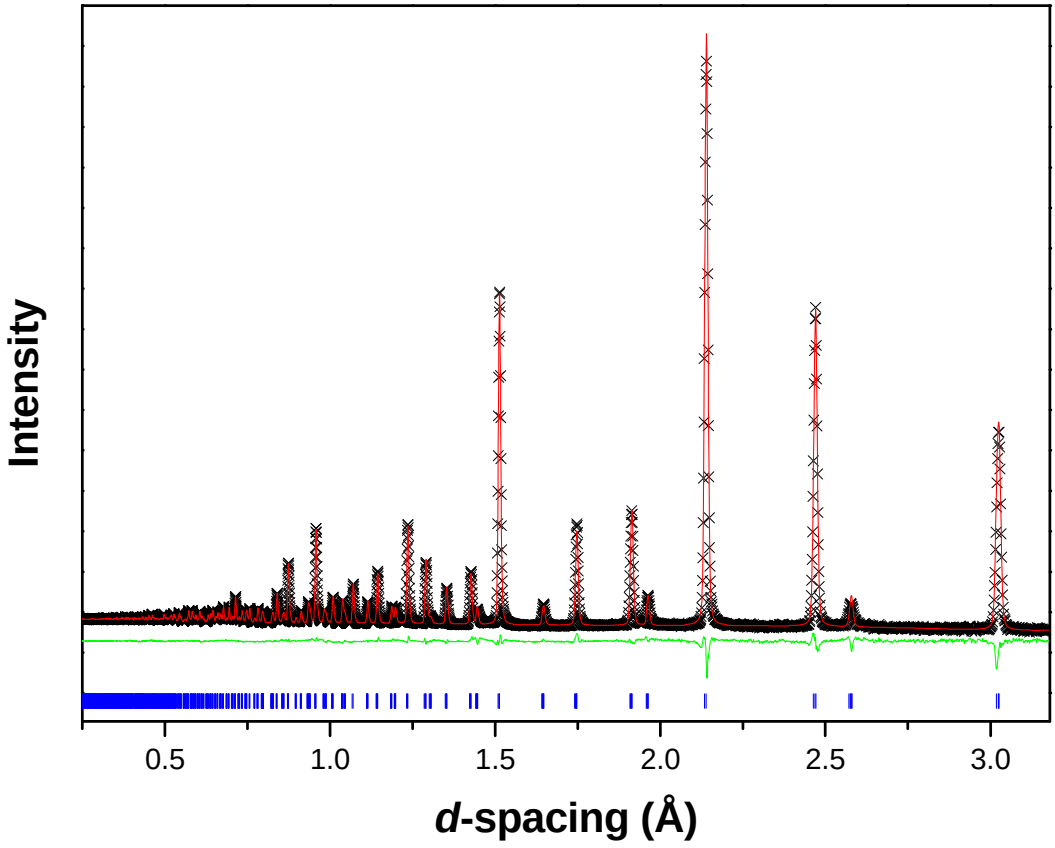

Figure 6.10: Neutron diffraction pattern of $Ba_2NdSn_{0.6}Sb_{0.4}O_{5.7}$ obtained at ambient temperature. The format is the same as for Figure 6.1

Table 6.2: Crystallographic information for the series $Ba_2NdSn_xSb_{1-x}O_{6-\delta}$ determined using neutron diffraction. Refinement of the x = 0.2 and 0.6 samples gives a Nd^{3+} occupancy of 0.95(2) and 0.81(1) for the 1*a* and 2*a* sites in these compounds, respectively, with the remainder of the sites consisting of B' cations.

Compound Space Group	Ba_2NdSbO_6 $R\bar{3}$	$Ba_2NdSn_{0.2}Sb_{0.8}O_{5.9}$ $R\bar{3}$	$Ba_2NdSn_{0.6}Sb_{0.4}O_{5.6}$ $I2/m$
a (Å)	6.02159(8)	6.03521(9)	6.0483(3)
b (Å)	= a	= a	6.0522(3)
c (Å)	= a	= a	8.5352(2)
α(°)	60.0968(4)	60.0512(5)	90
β(°)	= α	= α	90.192(3)
γ(°)	= α	= α	90
Ba	2*c* (x,x,x)	2*c* (x,x,x)	4*i* (x,0,z)
x	0.2520(3)	0.2494(9)	0.4962(9)
z	= x	= x	0.2555(8)
$U \times 10^{-2}$ (Å^2)	0.69(1)	0.65(1)	1.03(3)
Nd	1*a* (0,0,0)	1*a* (0,0,0)	2*a* (0,0,0)
$U \times 10^{-2}$ (Å^2)	0.39(1)	0.27(2)	0.28(2)
B'	1*b* (½,½,½)	1*b* (½,½,½)	2*d* (0,0,½)
$U \times 10^{-2}$ (Å^2)	0.19(1)	0.26(2)	0.38(2)
O1	6*f* (x,y,z)	6*f* (x,y,z)	4*i* (x,0,z)
x	0.7304(4)	0.7304(5)	-0.0276(8)
y	0.2408(1)	0.2409(1)	0
z	0.2963(1)	0.2942(2)	0.2673(3)
$U_{11} \times 10^{-2}$ (Å^2)	1.32(5)	0.88(5)	2.72(23)
$U_{22} \times 10^{-2}$ (Å^2)	1.36(4)	1.24(4)	4.58(40)
$U_{33} \times 10^{-2}$ (Å^2)	1.94(3)	1.67(4)	-0.31(3)
$U_{12} \times 10^{-2}$ (Å^2)	0.34(6)	0.39(5)	0
$U_{13} \times 10^{-2}$ (Å^2)	-0.24(6)	0.14(5)	0.37(10)
$U_{23} \times 10^{-2}$ (Å^2)	-1.52(3)	-1.20(4)	0
Occupancy	1	0.98	0.809(11)
O2			8*j* (x,y,z)
x			0.2666(9)
y			0.2575(12)
z			0.0122(4)
$U_{11} \times 10^{-2}$ (Å^2)			0.69(7)
$U_{22} \times 10^{-2}$ (Å^2)			1.55(11)
$U_{33} \times 10^{-2}$ (Å^2)			2.53(11)
$U_{12} \times 10^{-2}$ (Å^2)			-0.32(6)
$U_{13} \times 10^{-2}$ (Å^2)			-0.15(8)
$U_{23} \times 10^{-2}$ (Å^2)			0.34(14)
Occupancy			1.021(5)
R_p %	4.3	4.8	2.8
R_{wp} %	2.0	2.1	1.6
χ^2	5.9	1.8	5.6

Table 6.3: Bond lengths and bond valence sums (BVS) for selected compounds in the $Ba_2NdSn_xSb_{1-x}O_{6-\delta}$ series determined using neutron diffraction. In the case of the mixed Sn^{4+} and Sb^{5+} structures the BVS for Sn^{4+} is listed above Sb^{5+}. Bond valence sums account for the oxygen occupancies in each structure and in the *I*2/*m* structure, adopted by the x = 0.6 sample, the Ba-O1 and Ba-O2 bond lengths are listed in the second and third column respectively.

x	Ba-O			Nd-O		B'-O	
	Bond Length (Å)		BVS	Bond Length (Å)	BVS	Bond Length (Å)	BVS
0	3 × 2.8533(7) 3 × 2.988(4)	3 × 3.049(4) 3 × 3.1873(6)	1.76	6 × 2.2944(4)	3.71	6 × 1.9799(4)	5.42
0.2	3 × 2.8626(7) 3 × 3.020(12)	3 × 3.032(11) 3 × 3.184(1)	1.70	6 × 2.2902(5)	3.70	6 × 1.9912(5)	4.67 5.34
0.6	1 × 2.881(7) 2 × 3.0384(7) 1 × 3.170(7)	2 × 2.938(11) 2 × 2.942(8) 2 × 3.099(8) 2 × 3.119(11)	1.61	2 × 2.288(2) 4 × 2.245(2)	3.91	2 × 1.992(2) 4 × 2.039(2)	4.12 4.56

The decreased difference between the Nd-O and Sn/Sb-O bond lengths with increased Sn^{4+} doping is accompanied by a decrease in the degree of B-site cation ordering. While Ba_2NdSbO_6 is fully ordered refinements against X-ray diffraction patterns suggest that the B-site ordering decreases such that approximately 80 % of the 2*a* site is occupied by Nd^{3+} in $Ba_2NdSnO_{5.5}$. It should be noted that similarly to the $Ba_2LnSn_xSb_{1-x}O_{6-\delta}$ (Ln = Pr or Tb) series, described in Chapter 5, these refinements were carried out such that any disordering of the B-site cations involves both Sn^{4+} and Sb^{5+} replacing Nd^{3+} in a ratio consistent with the composition of the compound. As in the analogous Pr and Tb series this constraint is necessary because Sn^{4+} and Sb^{5+} have similar neutron scattering lengths and the same number of electrons, leading to very weak or no contrast in neutron and X-ray diffraction[23].

So far in this chapter it has been assumed that the number of oxygen vacancies in compounds in the series $Ba_2NdSn_xSb_{1-x}O_{6-\delta}$ should follow the relationship $\delta = \frac{x}{2}$. This assumes that the cations are present at their nominal stoichiometries and adopt their highest possible oxidation state. Initial refinement of the oxygen occupancies against neutron diffraction patterns, however, suggested that a higher than expected number of oxygen vacancies were present in all samples (for example contrast a δ of 0.34(1) determined from refinement against a neutron diffraction pattern of

$Ba_2NdSn_{0.2}Sb_{0.8}O_{6-\delta}$ to an expected δ of 0.10). Qualitative examination of the samples using X-ray Fluorescence spectroscopy confirms that the stoichiometry of each compound in the series is close to the nominal value.

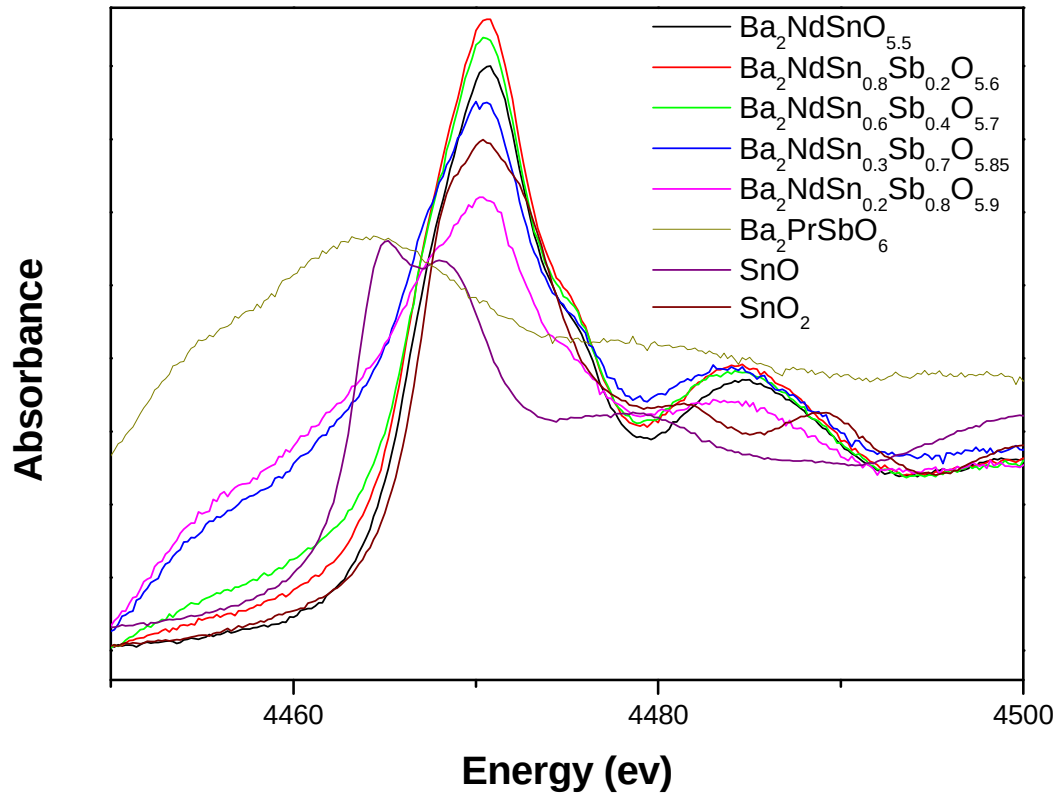

Figure 6.11: Sn L_I-edges of selected samples in the series $Ba_2NdSn_xSb_{1-x}O_{6-\delta}$ and, the Sn^{2+} and Sn^{4+} standards, SnO and SnO_2. The spectrum of Ba_2PrSbO_6 is also included as a reference for the features of the Sb L_{II} post-edge region that overlap with the Sn L_I-edge.

Consequently the oxidation states of cations in the series $Ba_2NdSn_xSb_{1-x}O_{6-\delta}$ were investigated to determine if a deviation from the expected oxygen stoichiometry was caused by the cations being in a lower oxidation state than expected. It was thought that Sn^{4+} and Sb^{5+} would be the only cations that might adopt lower than expected oxidation states since Ba^{2+} and Nd^{3+} are the only oxidation states found for Ba and Nd in most metal oxides[8]. X-ray Absorption Near-Edge Structure (XANES) spectroscopy was used to examine the Sn L_I- and L_{III}-edges and the Sb L_I-edge of selected compounds in the series $Ba_2NdSn_xSb_{1-x}O_{6-\delta}$. The Sn L-edge spectra show that Sn adopts the same oxidation state across the series with the only change evident in the regions examined being a feature near the L_I-edge caused by the overlap of this

edge with that of the Sb L_{II}-edge (see Figure 6.11). As found for the same edge in the $Ba_2LnSn_xSb_{1-x}O_{6-\delta}$ series, presented in Chapter 5, this feature increases in intensity with decreasing x as the ratio of Sb to Sn present in the sample increases and does not reflect any change in the oxidation state of Sn. The energy of the Sn L_I-edge of compounds in this series is close to that of the Sn^{4+} standard, SnO_2, and there is no features common to that of the Sn^{2+} standard, SnO. The XANES spectra indicate that Sn^{4+} is the only oxidation state of Sn present in this series of compounds.

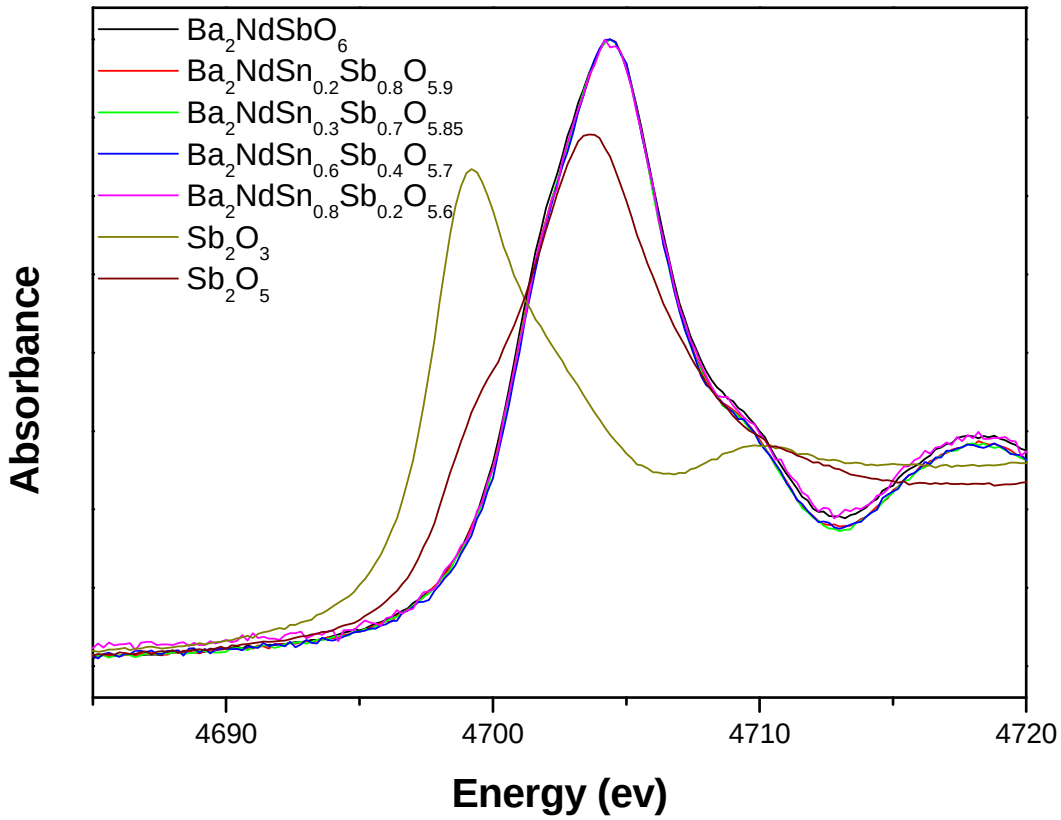

Figure 6.12: Sb L_I-edges of selected samples in the series $Ba_2NdSn_xSb_{1-x}O_{6-\delta}$ and, the Sb^{3+} and Sb^{5+} standards, Sb_2O_3 and Sb_2O_5.

Similarly the Sb-L_I edges of compounds in the series $Ba_2NdSn_xSb_{1-x}O_{6-\delta}$ do not change with increasing Sn^{4+} doping and are slightly higher in energy than that of the Sb^{5+} standard, Sb_2O_5 (see Figure 6.12). There are no features in the XANES spectra of these compounds matching those of the Sb^{3+} standard, Sb_2O_3 and it can be concluded that Sb in the series $Ba_2NdSn_xSb_{1-x}O_{6-\delta}$ is only present in the pentavalent state. Since it has been shown that the stoichiometry of these compounds is consistent with the nominal value and the cations in the series $Ba_2NdSn_xSb_{1-x}O_{6-\delta}$ adopt their highest

possible oxidation state the excessive number of oxygen vacancies indicated by neutron diffraction must be incorrect. This error most likely arises from the correlation between the oxygen occupancies and displacement parameters. Refinements were subsequently carried out such that the total oxygen vacancies present were fixed according to the relationship $\delta = \frac{x}{2}$. The introduction of this constraint did not significantly change the quality of the fit of the models to the neutron diffraction patterns (cf. a χ^2 of 1.8 for a constrained fit to the neutron diffraction pattern of $Ba_2NdSn_{0.2}Sb_{0.8}O_{5.9}$ to 1.7 for an unconstrained fit).

Refinement of the occupancy of the two oxygen anion sites in the monoclinic structures adopted by the compounds with x = 0.6 and 0.8 showed that, at ambient temperature, the oxygen vacancies are concentrated onto the axial, 4*i*, oxygen site while the equatorial, 8*j*, site is effectively fully occupied. In $Ba_2NdSn_{0.6}Sb_{0.4}O_{5.7}$ the axial and equatorial oxygen sites are 81(1) % and 102.1(5) % occupied, respectively, while in $Ba_2NdSn_{0.8}Sb_{0.2}O_{5.6}$ the axial and equatorial oxygen sites are 84(2) % and 98(1) % full. Having established that oxygen vacancies are located on the axial site in both these samples at room temperature it was of interest to explore whether such oxygen vacancy ordering persists below ambient temperature, where the lowest energy form of oxygen ordering in these compounds would be expected to be adopted, and above room temperature where perovskites with oxygen vacancies are of interest for application in solid oxide fuel cells. Refinement of the oxygen occupancies of $Ba_2NdSn_{0.4}Sb_{0.6}O_{5.7}$ using a neutron diffraction pattern collected at -269 °C (4 K) indicated that the oxygen vacancies remain ordered onto the axial site at low temperature confirming that this is the lowest energy form of oxygen vacancy ordering in this compound (see Figure 6.13).

Above room temperature refinements show that the oxygen vacancy ordering in $Ba_2NdSn_{0.6}Sb_{0.4}O_{6-\delta}$ reverses such that the vacancies are concentrated onto the equatorial site at temperatures above 300 °C (see Figure 6.13). Previous studies have found that oxygen vacancies in most perovskites that adopt a structure with more than one crystallographic oxygen atom site, including $BaLn_xCe_{1-x}O_{6-\delta}$[13], $Sr_xLn_{1-x}GaO_{3-\delta}$[10] and $Sr_xLn_{1-x}CoO_{3-\delta}$[11, 12], are concentrated onto the equatorial sites. Therefore the

change in oxygen vacancy ordering to this site at higher temperatures is not surprising. This is apparently the first example where a temperature dependency of oxygen vacancy ordering has been established in a double perovskite and it is important to conduct further studies of other compounds adopting this structure to establish if this is a general effect.

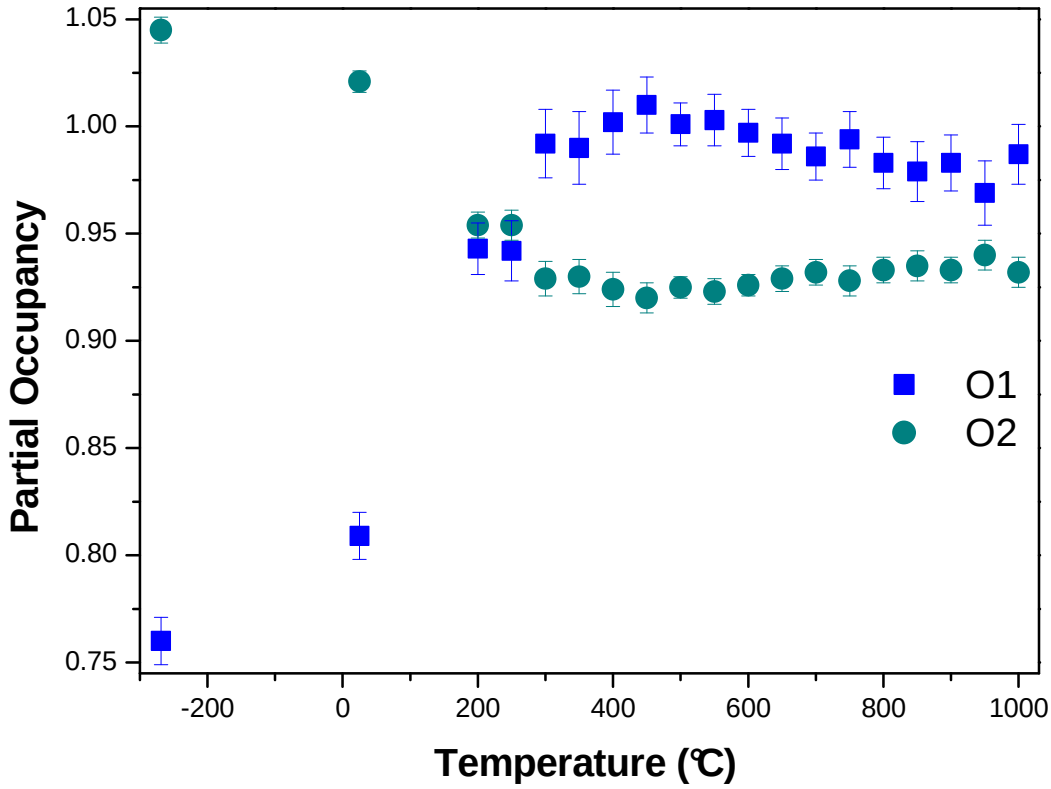

Figure 6.13: Oxygen occupancies of $Ba_2NdSn_{0.6}Sb_{0.4}O_{5.7}$ determined at various temperatures using neutron diffraction. O1 and O2 represent the 4*i* and 8*j*, axial and equatorial, oxygen atom sites respectively.

There is an obvious anomaly in the thermal expansion of the unit cell of $Ba_2NdSn_{0.6}Sb_{0.4}O_{5.7}$ near 300 °C. This is the same temperature at which the reversal of oxygen vacancy ordering from the 4*i* to the 8*j* site occurs (see Figure 6.14). Between 250 and 350 °C the monoclinic distortion decreases before increasing gradually again at higher temperatures. The out-of-phase octahedral tilt around the (110) axis has also been found to decrease to zero at approximately the same temperature. The tilt angle was found to decrease from 5.4(3)° at -269 °C to 4.0(2)° at ambient temperature and then to approximately 0.5° between 200 and 400 °C, above which it is effectively zero. Removal of the octahedral tilting from a double

perovskite would typically lead to a transition to the untilted $Fm\bar{3}m$ cubic structure. In the present case a significant monoclinic distortion persists at all temperatures examined (see Figure 6.14 and 6.15 for a plot of the variable temperature lattice parameters and a typical high temperature diffraction pattern of $Ba_2NdSn_{0.4}Sb_{0.6}O_{5.7}$, respectively) and the fit of the monoclinic symmetry to the diffraction patterns is superior to higher symmetry double perovskite structures at even the highest temperature studied (cf. a χ^2 of 2.3 for a fit with $I2/m$ symmetry to the pattern obtained at 1000 °C to 4.2, 4.2 and 4.5 for structures in $I4/m$, $R\bar{3}$ and $Fm\bar{3}m$).

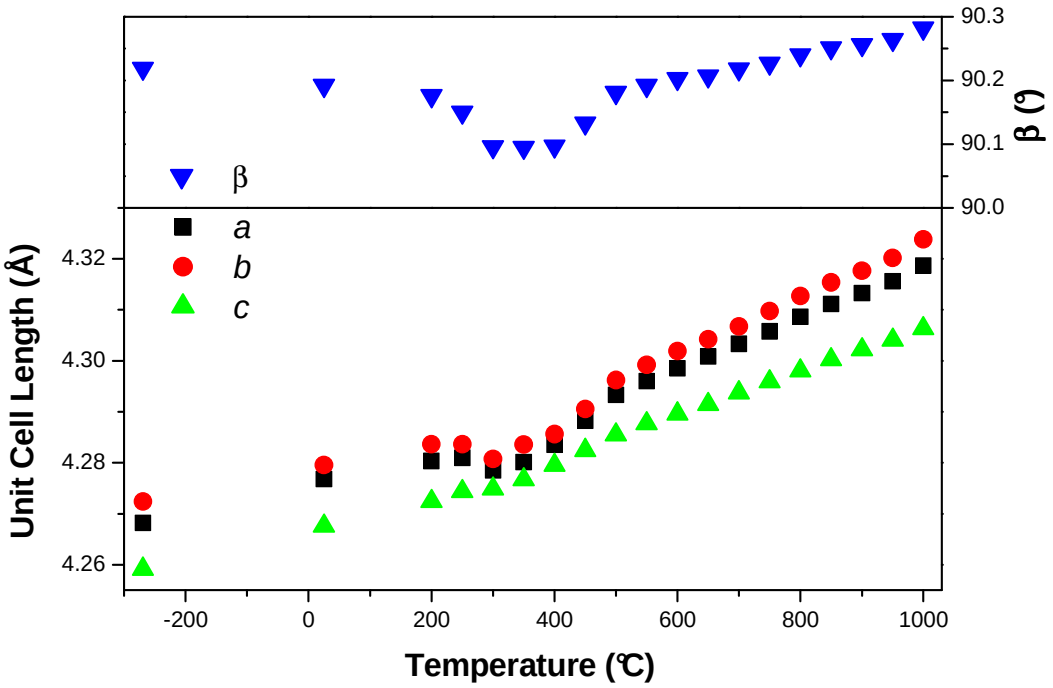

Figure 6.14: Reduced lattice parameters of $Ba_2NdSn_{0.6}Sb_{0.4}O_{5.7}$ versus temperature.

That the monoclinic structure persists beyond the temperature where the octahedral tilting is lost suggests that the oxygen vacancy ordering plays a significant role in the adoption of monoclinic symmetry. The oxygen vacancy ordering may also be the cause of the *b*-axis being longer than the *a*-axis which, as mentioned previously, is unusual for perovskites with the $I2/m$ structure. It is also possible that a different monoclinic symmetry, consistent with this type of oxygen vacancy ordering but without octahedral tilting, may be adopted by $Ba_2NdSn_{0.6}Sb_{0.4}O_{5.7}$ above 300 °C. The fit in $I2/m$ is, however, excellent and there are no additional reflections suggestive of an alternate symmetry. Group theoretical analysis was carried out, in conjunction with

this work, by Christopher Howard at ANSTO using the program ISOTROPY[24] to identify if there were any other possible monoclinic structures which had oxygen vacancy ordering but no octahedral tilting. This analysis indicated that *I*2/*m* was the only monoclinic symmetry adopted by perovskites distorted from the cubic double perovskite structure by oxygen vacancy ordering of the type found in this work, with or without the presence of out-of-phase octahedral tilting. These conditions were placed on the group theoretical analysis because only *R*-point super-lattice reflections were present in diffraction patterns of $Ba_2NdSn_{0.6}Sb_{0.4}O_{5.7}$ which, as discussed in Chapter 2, reveal the presence of B-site cation ordering and/or octahedral tilting. Unfortunately there are no additional reflections that allow direction discrimination of the *I*2/*m* monoclinic structure from an untilted double perovskite structure. It is consequently considered that *I*2/*m* is the correct symmetry for $Ba_2NdSn_{0.6}Sb_{0.4}O_{5.7}$ at all temperatures examined despite the absence of any detectable octahedral tilting at higher temperatures.

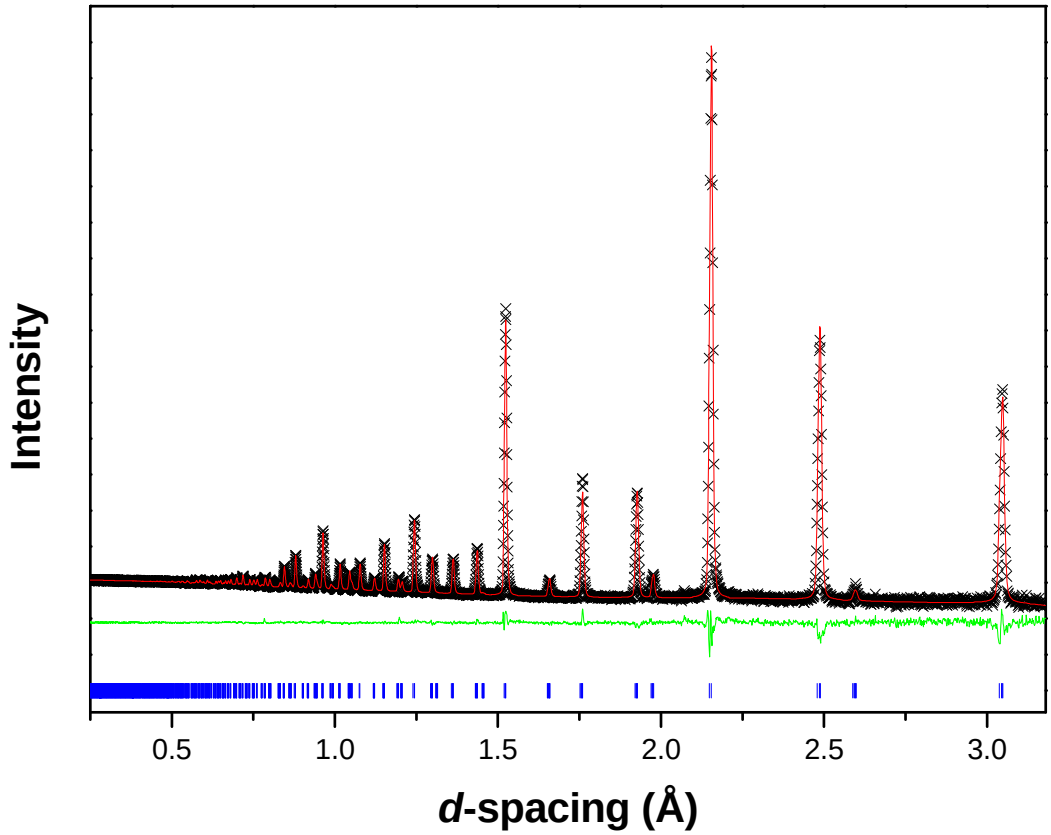

Figure 6.15: A neutron diffraction pattern of $Ba_2NdSn_{0.6}Sb_{0.4}O_{5.7}$ collected at 750 °C fitted with *I*2/*m* symmetry. The quality of the fit is typical of the high temperature patterns of this sample and the format is the same as for Figure 6.1.

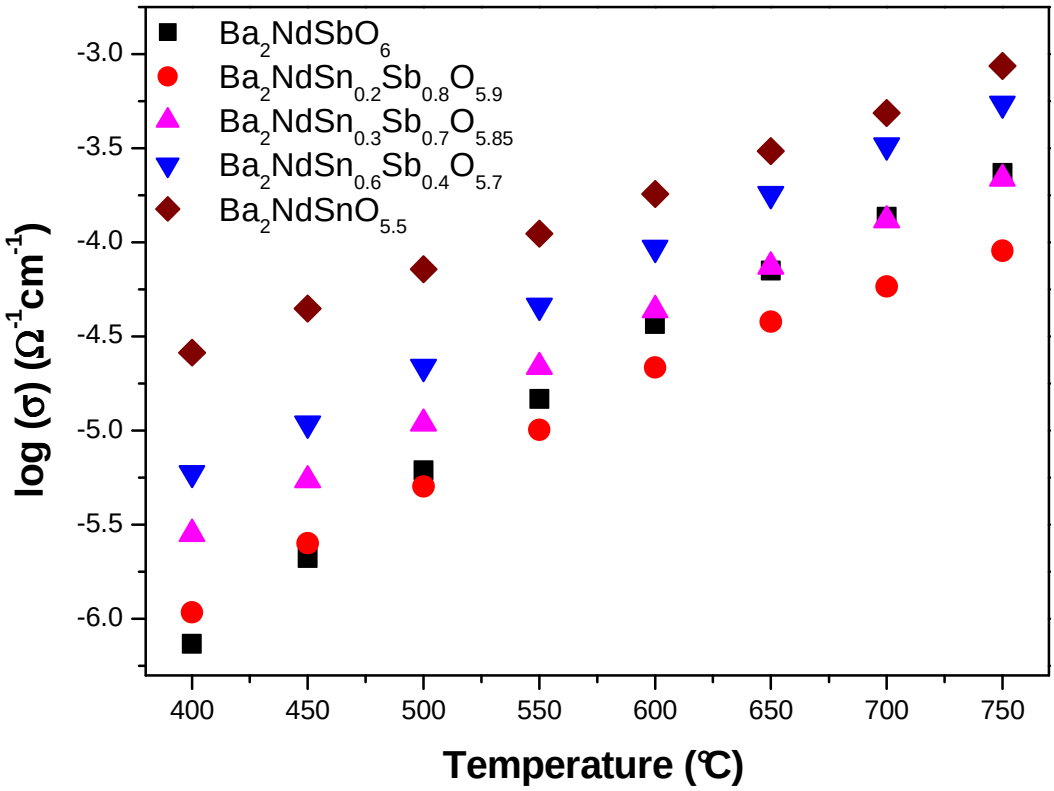

Figure 6.16: Conductivity in air versus temperature for samples in the series $Ba_2NdSn_xSb_{1-x}O_{6-\delta}$.

Having thoroughly examined the structures adopted by compounds in the series $Ba_2NdSn_xSb_{1-x}O_{6-\delta}$ impedance spectroscopy was used to characterise the bulk conductivity of these materials in air (see Figure 6.16). These data were collected by Nathan Webster at the University of Western Australia. By analogy with $Ba_2YSnO_{5.5}$ the measured conductivity can be interpreted as being a mixture of ionic and electronic conductivity, with the later being caused by electronic holes formed from the filling of oxygen vacancies[6]. Unfortunately we were unable to discriminate between these types of conductivity because the atmosphere in which the measurements were carried out could not be controlled. Despite this limitation it can be seen that conductivity at 400 °C, the lowest temperature examined, increases as the number of oxygen vacancies present becomes larger. $Ba_2NdSnO_{5.5}$ has much higher conductivity than the other samples examined at this temperature. The rate at which the conductivity of Ba_2NdSbO_6 increases with temperature, is significantly faster than for the compounds with x = 0.2 and 0.3 suggesting that a small amount of Sn^{4+} doping may have an unfavourable impact on overall conductivity. The conductivity of

$Ba_2NdSn_{0.6}Sb_{0.4}O_{5.7}$ also increases at a faster rate with temperature than that of other samples studied. This leads to its conductivity approaching that of $Ba_2NdSnO_{5.5}$ at the highest temperatures examined. It is speculated that the relatively slow increase in the conductivity of $Ba_2NdSnO_{5.5}$ with increasing temperature may be caused by the presence of a significant amount of strain in this material, as indicated by the neutron diffraction patterns, and that local strain acts as an additional barrier to oxygen mobility. $Ba_2NdSn_{0.6}Sb_{0.4}O_{5.7}$ and $Ba_2NdSnO_{5.5}$ appear to have similar conductivity to $Ba_2YSnO_{5.5}$ in air suggesting that their conductivity is worthy of further study[6].

6.5 Conclusions

The structures of compounds in the series $Ba_2NdSn_xSb_{1-x}O_{6-\delta}$ have been examined using synchrotron X-ray and neutron diffraction. It has been found that this series undergoes a transformation from $R\bar{3}$ rhombohedral to $I2/m$ symmetry via a two phase region caused by phase segregation. An unusual contraction in the lattice parameters of $Ba_2NdSnO_{5.5}$ was found upon heating over a temperature range of 250 to 500 °C. This behaviour was not, however, observed on cooling and is a consequence of the loss of water from the crystal structure of this material, a promising indication of possible proton conductivity.

XANES spectra of the Sn L_I- and Sn L_{III}-edges and Sb L_I-edge were used to verify that, in the series $Ba_2NdSn_xSb_{1-x}O_{6-\delta}$, the Sn and Sb cations are tetravalent and pentavalent respectively. This confirmed that the number of oxygen vacancies in the compounds in the series $Ba_2NdSn_xSb_{1-x}O_{6-\delta}$ follows the relationship $\delta = \frac{x}{2}$. It was found that the oxygen vacancies in $Ba_2NdSn_{0.6}Sb_{0.4}O_{5.7}$ and $Ba_2NdSn_{0.8}Sb_{0.2}O_{5.6}$ concentrate onto the axial site at room temperature but variable temperature neutron diffraction indicates that the vacancies in the former sample change to concentrating on the equatorial site above 300 °C. This change in oxygen vacancy ordering is accompanied by an initial decrease in the monoclinic distortion, which then increases again at higher temperatures. This is the first time that a reversal of oxygen vacancy ordering with increasing temperature has been found in a double perovskite. Examination of the conductivity of these compounds in air suggests that, in general,

the total bulk conductivity of these materials increases in those samples with more oxygen vacancies. It is, however, suggested that the local strains in $Ba_2NdSnO_{5.5}$, caused by the large number of oxygen vacancies in this sample, reduce the rate at which conductivity increases with increasing temperature.

6.6 References

[1] J.B. Goodenough, Rep. Prog. Phys. 67 (2004) 1915-1993.

[2] V.V. Kharton, F.M.B. Marques, A. Atkinson, Solid State Ionics 174 (2004) 135-149.

[3] K.D. Kreuer, Solid State Ionics 97 (1997) 1-15.

[4] S.J. Skinner, Int. J. Inorg. Mater. 3 (2001) 113-121.

[5] N. Bonanos, K.S. Knight, B. Ellis, Solid State Ionics 79 (1995) 161-170.

[6] P. Murugaraj, K.D. Kreuer, T. He, T. Schober, J. Maier, Solid State Ionics 98 (1997) 1-6.

[7] T. Norby, Nature 410 (2001) 877-878.

[8] H.J. Emeléus, A.G. Sharpe, *Modern Aspects of Inorganic Chemistry*, Routledge & Kegan Paul, London, 1973.

[9] R.D. Shannon, Acta Cryst. A 32 (1976) 751-767.

[10] M. Kajitani, M. Matsuda, A. Hoshikawa, S. Harjo, T. Kamiyama, T. Ishigaki, F. Izumi, M. Miyake, Chem. Mater. 17 (2005) 4235-4243.

[11] M. James, D. Cassidy, D.J. Goossens, R.L. Withers, J. Solid State Chem. 177 (2004) 1886-1895.

[12] R.L. Withers, M. James, D.J. Goossens, J. Solid State Chem. 174 (2003) 198-208.

[13] K.S. Knight, Solid State Ionics 145 (2001) 275-294.

[14] Q. Zhou, B.J. Kennedy, M.M. Elcombe, J. Solid State Chem. 180 (2007) 541-548.

[15] Q. Zhou, B.J. Kennedy, C.J. Howard, M.M. Elcombe, A.J. Studer, Chem. Mater. 17 (2005) 5357-5365.

[16] C.J. Howard, B.J. Kennedy, P.M. Woodward, Acta Cryst. B 59 (2003) 463-471.

[17] K.S. Knight, Solid State Ionics 127 (2000) 43-48.

[18] T. Ito, T. Nagasaki, K. Iwasaki, M. Yoshino, T. Matsui, H. Fukazawa, N. Igawa, Y. Ishii, Solid State Ionics 178 (2007) 607-613.

[19] T. Ito, T. Nagasaki, K. Iwasaki, M. Yoshino, T. Matsui, N. Igawa, Y. Ishii, Solid State Ionics 177 (2006) 2353-2356.

[20] T. Ito, T. Nagasaki, K. Iwasaki, M. Yoshino, T. Matsui, N. Igawa, Y. Ishii, Solid State Ionics 178 (2007) 13-17.

[21] I. Sosnowska, R. Przenioslo, W. Schäfer, W. Kockelmann, R. Hempelmann, K. Wysocki, J. Alloys Compd. 328 (2001) 226-230.

[22] T. Shimoyama, T. Tojo, H. Kawaji, T. Atake, N. Igawa, Y. Ishii, Solid State Ionics 179 (2008) 231-235.

[23] V.F. Sears, Neutron News 3 (1992) 26-37.

[24] H.T. Stokes, D.M. Hatch, B.J. Campbell, ISOTROPY. http://stokes.byu.edu/isotropy.html (21/05/2008).